Journal of Materials Chemistry A

Stable High Current Density Operation of $La_{0.6}Sr_{0.4}Co_{0.2}Fe_{0.8}O_{3-\delta}$ Oxygen Electrodes

Journal:	*Journal of Materials Chemistry A*
Manuscript ID	TA-ART-04-2019-004020.R1
Article Type:	Paper
Date Submitted by the Author:	07-May-2019
Complete List of Authors:	Lu, Matthew; Northwestern University, Materials Science and Engineering Railsback, Justin; Northwestern University, Materials Science and Engineering Wang, Hongqian; Northwestern University, Materials Science and Engineering Liu, Qinyuan; Northwestern University, Materials Science and Engineering Chart, Yvonne; Northwestern University, Materials Science and Engineering Zhang, Shanlin; Xi'an Jiaotong University, State Key Laboratory for Mechanical Behavior of Materials, School of Materials Science and Engineering; Northwestern University, Materials Science and Engineering Barnett, Scott; Northwestern University, Materials Science and Engineering

Stable High Current Density Operation of $La_{0.6}Sr_{0.4}Co_{0.2}Fe_{0.8}O_{3-\delta}$ Oxygen Electrodes

Matthew Y. Lu, Justin G. Railsback, Hongqian Wang, Qinyuan Liu, Yvonne A. Chart, Shan-Lin Zhang,† and Scott A. Barnett*

Department of Materials Science and Engineering, Northwestern University, Evanston, Illinois 60208, USA

†Current Address: State Key Laboratory for Mechanical Behavior of Materials, School of Materials Science and Engineering, Xi'an Jiaotong University, Xi'an, Shaanxi, 710049, People's Republic of China

*Corresponding author. E-mail: s-barnett@northwestern.edu

Abstract

Solid oxide cells operated reversibly between fuel cell and electrolysis modes are promising for energy storage with extremely high capacity. $La_{0.6}Sr_{0.4}Co_{0.2}Fe_{0.8}O_{3-\delta}$ (LSCF) has become the dominant oxygen electrode material in electrolysis and reversible operation. However, LSCF has been widely reported to degrade due to Sr surface segregation. The present understanding is that the segregation rate and hence the degradation rate increases with increasing temperature and current density. Here we present a study of LSCF electrode performance and stability carried out with a series of extended life tests (1000 hours) over a range of temperatures and reversing current densities. Although the results at lower temperatures (650 – 700 °C) show the expected increase in segregation-induced degradation with increasing current density, at higher temperature (750 °C) stability is improved and the electrodes become fully stable at the highest current density of 1.5 A cm^{-2}, maintaining a stable polarization resistance of 0.08 $\Omega \cdot cm^2$. This unexpected result is explained by the increased electrochemical

activity of LSCF at the higher temperature and a very rapid development of a stable surface segregated Sr layer.

Main Text

The rapid increase in utilization of intermittent renewable energy sources, as needed to mitigate global warming,[1] will give rise to an increasing need for electricity storage.[2,3] The time frame for storage is over days or longer, requiring clean technologies with large energy storage capacities. Solid oxide cells (SOCs) operated as electrolyzers provide a promising and scalable method for efficiently converting electricity into renewable fuels for direct utilization, e.g., for transportation. The fuels can also be stored and converted back to electricity by reversing SOC operation to fuel cell mode, completing an electricity storage cycle with the requisite very high energy storage capacity along with relatively low cost and high efficiency.[4–6] Although SOCs have been extensively developed for fuel cell applications and proven to provide good stability, much higher degradation rates are often observed during electrolysis and reversible operation, particularly at higher current densities.[7–9] Voltage degradation rates (at constant current) are often well above 1 %/kilohour, much higher than that needed for the device to operate effectively over economically-viable operational lifetimes of $\geq$ 5 years.[4,10]

Early studies of solid oxide electrolysis utilized cells with the $(La_{0.8}Sr_{0.2})_{0.98}MnO_3$ (LSM) -YSZ oxygen electrode; however, these electrodes were shown to fail at relatively large current densities ($\gtrsim$ 0.5 $A \cdot cm^{-2}$) via oxygen bubble formation, crack formation, and delamination at or near the electrode-electrolyte interface.[11–15] More recent electrolysis studies have focused on SOCs with mixed ionic and electronic conducting (MIEC) oxygen electrodes such as $La_{0.6}Sr_{0.4}Co_{0.2}Fe_{0.8}O_{3-\delta}$ (LSCF) that yield better performance and electrolysis stability.[16,17] While LSCF and other similar ABO_3 perovskite MIEC electrodes typically do not degrade by the

aforementioned mechanisms, they can degrade via a different mechanism–surface segregation of an A-site cation (typically Sr) that blocks electrochemically active sites for oxygen adsorption and electron transfer.[9,18–21] The rate of Sr segregation generally increases with increasing temperature, and the current/overpotential during cell operation can also impact segregation, although there are sometimes conflicting results on the effects of anodic versus cathodic polarization.[21–29]

In contrast to the above mentioned findings, that typically show substantial degradation, many of which were obtained with model thin film electrodes, porous LSCF electrodes used in long-term SOC lab-scale and stack tests have generally shown little electrode degradation.[16,30–34] This disconnect may be related to the different operating conditions (temperature, current density, and overpotential) or electrode geometries (thin film versus porous). These conflicting results suggest that a comprehensive study, focusing on porous electrodes over a range of operating temperatures and current densities, is needed to understand LSCF degradation and find operating conditions that yield stable operation.

Here we describe life test results detailing the effects of reversing current density (j) and temperature on the electrochemical stability of porous LSCF electrodes. The study directly correlates the evolution of electrochemical performance, measured using impedance spectroscopy, with quantitative 3D tomographic microstructure observations and Sr segregation measurements. A novel surface cleaning experiment is used to prove the direct correlation between Sr segregation and electrochemical performance degradation. A key finding is the unexpected observation of stable operation at relatively high current density (j = 1.5 A·cm^{-2}) and temperature (750 ^{o}C). The results show how LSCF electrodes can be operated reversibly at

desirably high current density without significant degradation; the results may also be applicable to electrolysis operation, since the degradation mechanisms are typically similar.[11,35,36]

Electrochemical Characterization

Figure 1 shows voltage versus time during life tests carried out at 650 and 750 °C, both with j = 1.5 A·cm^{-2}. The cycle used in these experiments, with 6 hours in electrolysis mode and 6 hours in fuel cell mode, simulates the conditions at the SOC oxygen electrode during a reversible energy storage application. As expected, the cell voltage is higher at the lower temperature. During the 650 °C test, the voltage increases rapidly initially but then more slowly later in the life test. The voltage evolution over time trends differently in the 750 °C test, with an initial decrease early in the test followed by stable operation.

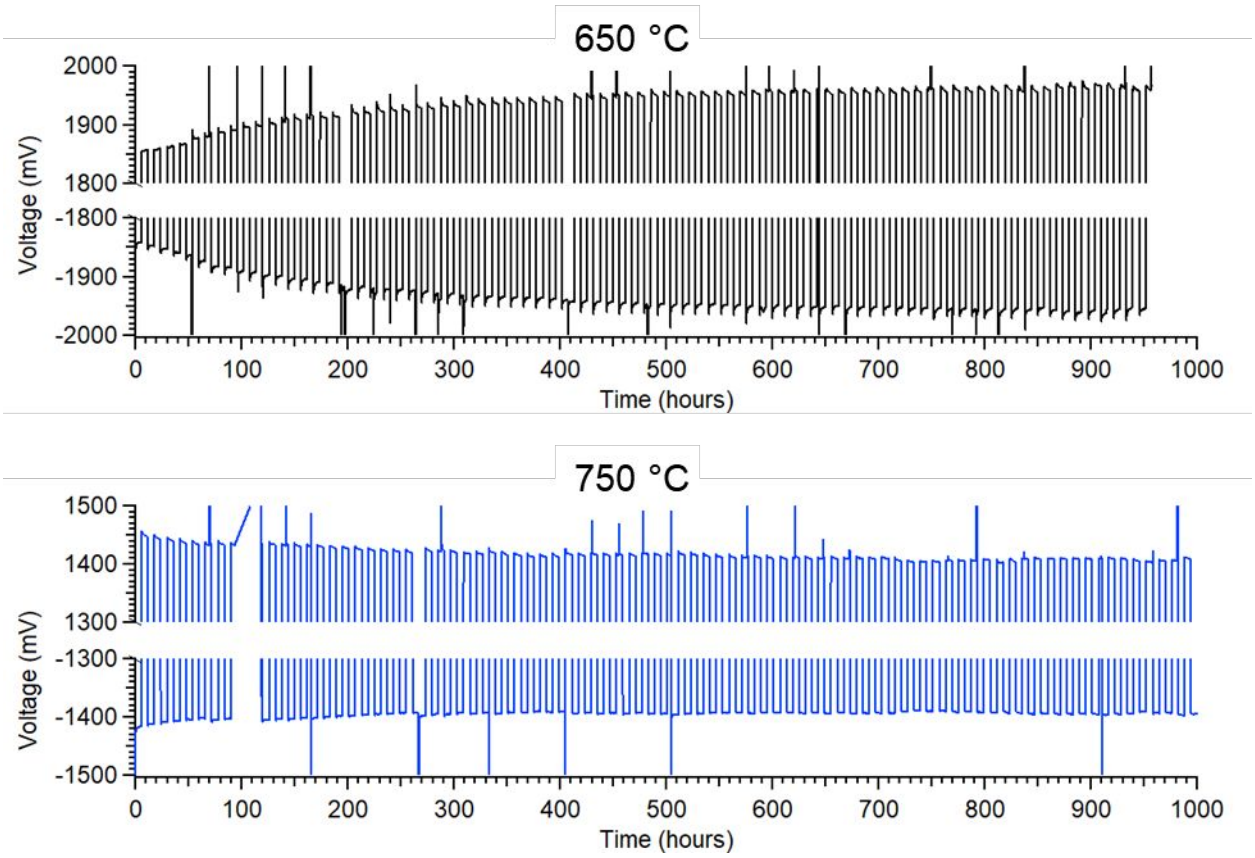

Fig. 1 | Voltage data for LSCF |GDC|LSCF life tests. Cells are operated for ~ 1000 hours at j = 1.5 A·cm^{-2} at 650 °C and 750 °C

Figure 2 shows typical impedance spectra taken at 0, 240, and 990 hours during the life test at 650 °C with j = 1.5 A·cm^{-2}. The spectra are fit with an *L*-*R*-*RQ*-*G* equivalent circuit that is widely used to fit data for mixed ionic and electronic conducting electrodes such as LSCF.[37–39] The *RQ* element is attributed to charge transfer resistance at the electrode-electrolyte interface whereas the Gerischer element (*G*) is attributed to co-limiting oxygen surface exchange and diffusion in LSCF, and the sum of the two is the total polarization resistance, R_P.[19,29,40–43] The *L* element accounts for measurement circuit inductance, and *R* corresponds to the ohmic resistance, or effectively the electrolyte resistance. The high frequency intercept shifts very little, indicating no significant change in *R*. On the other hand, the increase in the magnitude of the impedance

response demonstrates that there is substantial electrode degradation. From the evolution of the impedance spectra, the increase in the cell resistance is primarily associated with the low-frequency Gerischer response. Note that the impedance spectra taken at 750 °C (Supplementary Fig. 1) have the same basic form as those at 650 °C and are fit well using the same equivalent circuit; however, the resistance values are smaller and the spectra change little during the life test.

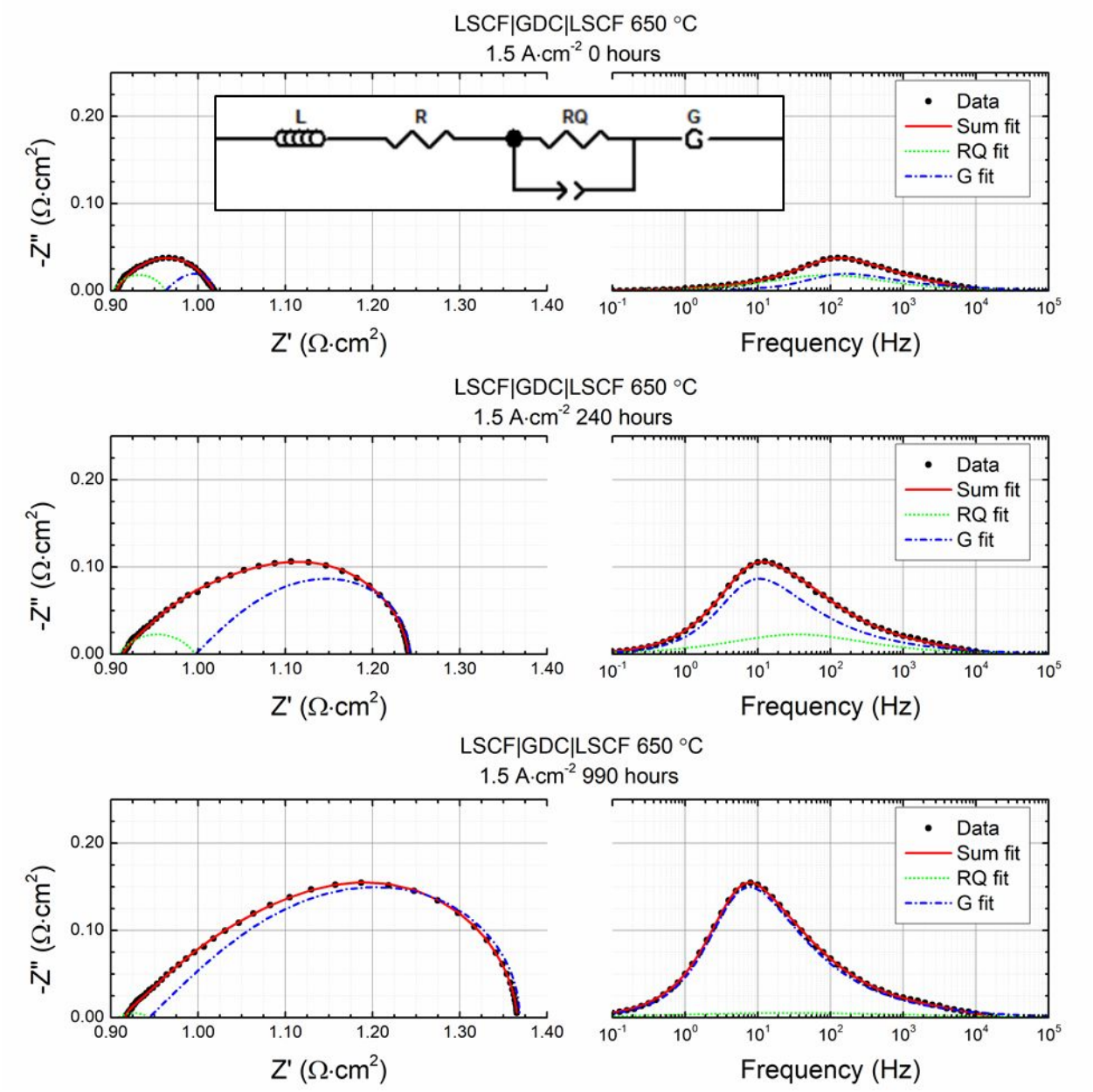

Fig. 2 | Evolution of Nyquist and Bode plots for LSCF|GDC|LSCF cells. Impedance spectra are shown at 0, 240, and 990 hours during operation at 650 °C and j = 1.5 A·cm^{-2}. An inset of the L-R-RQ-G equivalent circuit model used for fitting is shown.

The equivalent circuit fits are used to obtain R and R_P values that are plotted in Figure 3. At both 650 °C (Figure 3a) and 750 °C (Figure 3b), R is stable at all j. Several cells exhibit slight improvements in R, but the magnitudes of these changes are relatively insignificant, ~ 0.01

103 Ω·cm^2, similar to prior results for LSCF-based cells.[9,19] The cell-to-cell variations in ohmic
104 resistance result from differing electrolyte thicknesses.

105 At 650 °C (Figure 3c), the degradation rate of R_P increases with increasing j up to 1.0
106 A·cm^{-2}. At j = 1.5 A·cm^{-2}, R_P degrades rapidly at the start, but the degradation rate slows
107 throughout the 1000 hour test. These results are similar to those reported previously for similar
108 LSCF electrodes tested at 700 °C.[9] The significant R_P increases at both 650 and 700 °C can be
109 explained by Sr surface segregation.[9,19,44,45] At 750 °C (Figure 3d) and j = 0, 0.7, and 1.0 A·cm^{-2},
110 R_P again increases rapidly over the first ~ 150 hours, and increases very slowly thereafter.
111 However, when j = 1.5 A·cm^{-2}, R_P becomes remarkably stable throughout the life test.

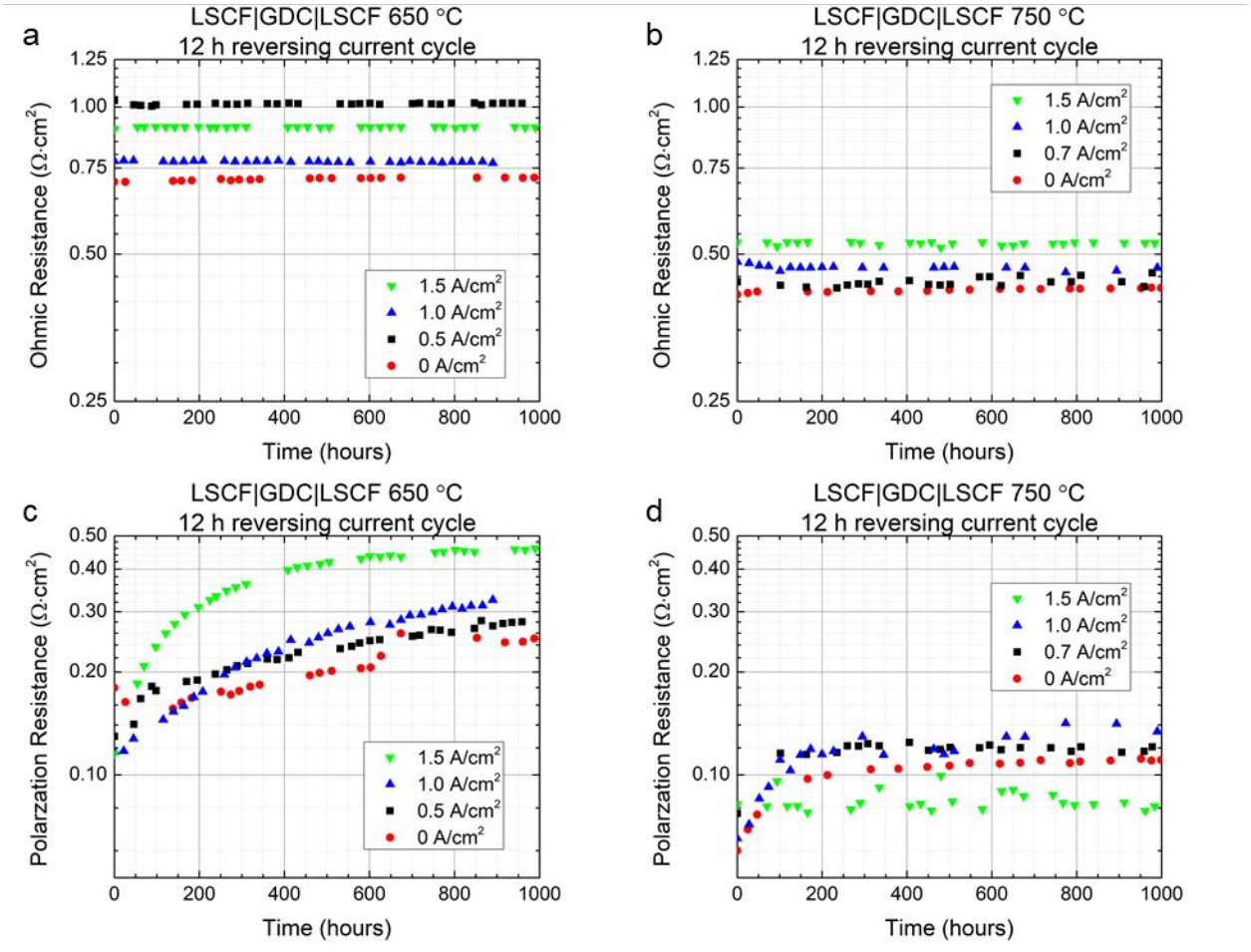

112

Fig. 3 | Ohmic and polarization resistances for LSCF|GDC|LSCF cells during ~ 1000 hour life tests. Current densities range from $j = 0$ to 1.5 A·cm^{-2} with 650 °C plotted on the left (**a,c**), 750 °C (**b,d**) on the right.

Figure 4 shows the effect of temperature on R_P separated into its two components: the interfacial RQ resistance (R_I) and the Gerischer resistance (R_G). Note that the 700 °C data is from previous work and refitted using ravdav software to deconvolute the contributions from the RQ and Gerischer resistances.[9,46] R_I remains stable or decreases slightly with time in almost all cases, whereas R_G is either stable or saturates after an initial increase.[19] At $j = 0$ (Figure 4b), R_G remains stable at 650 °C, but increases with time at the higher temperatures. At $j = 1.5$ A·cm^{-2} (Figure 4d), R_G remains constant at 750 °C, but increases substantially at lower temperatures. These opposing temperature dependences at different j are explained below based on structural and chemical characterization.

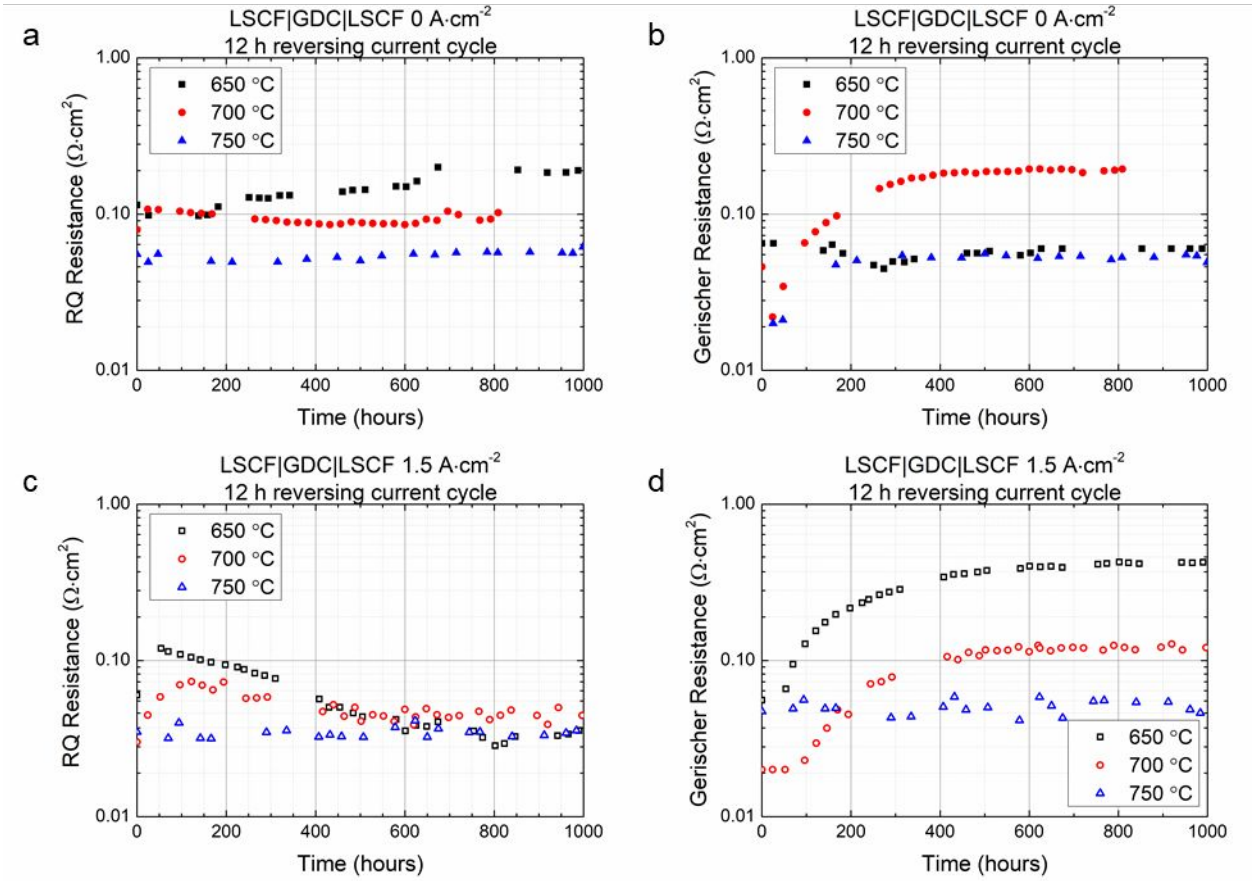

Fig. 4 | *RQ* and Gerischer resistances for LSCF|GDC|LSCF cells. a,c, *RQ* resistance and **b,d**, Gerischer resistance during life tests at various temperatures in ambient air. The top row (**a,b**) shows life tests with no current (j = 0 A·cm^{-2}) and the bottom row (**c,d**) shows reversing current life tests with j = 1.5 A·cm^{-2} .

Microstructural Characterization

Figure 5 shows scanning electron microscope (SEM) images of the region near the electrode-electrolyte interface of the untested control cell (Figure 5a) compared with cells after life testing at j = 1.5 A·cm^{-2} at 650 °C (Figure 5b) and at 750 °C (Figure 5c). There is no discernable difference between the microstructures; that is, life testing at high current density yielded no significant microstructures changes either for the highest degradation case (650 °C) or

the stable operation case (750 °C). Figure 5d shows an energy dispersive X-ray spectroscopy (EDS) linescan of the electrode-electrolyte interface for the 750 °C and j = 1.5 A·cm^{-2} cell. Although there is apparent interfacial broadening of ~ 1 μm, a similar width is observed in all cells (not shown here) that can be attributed to the limited spatial resolution of the EDS measurement.[41] Thus, no elemental migration is detected at the spatial resolution of SEM-EDS.

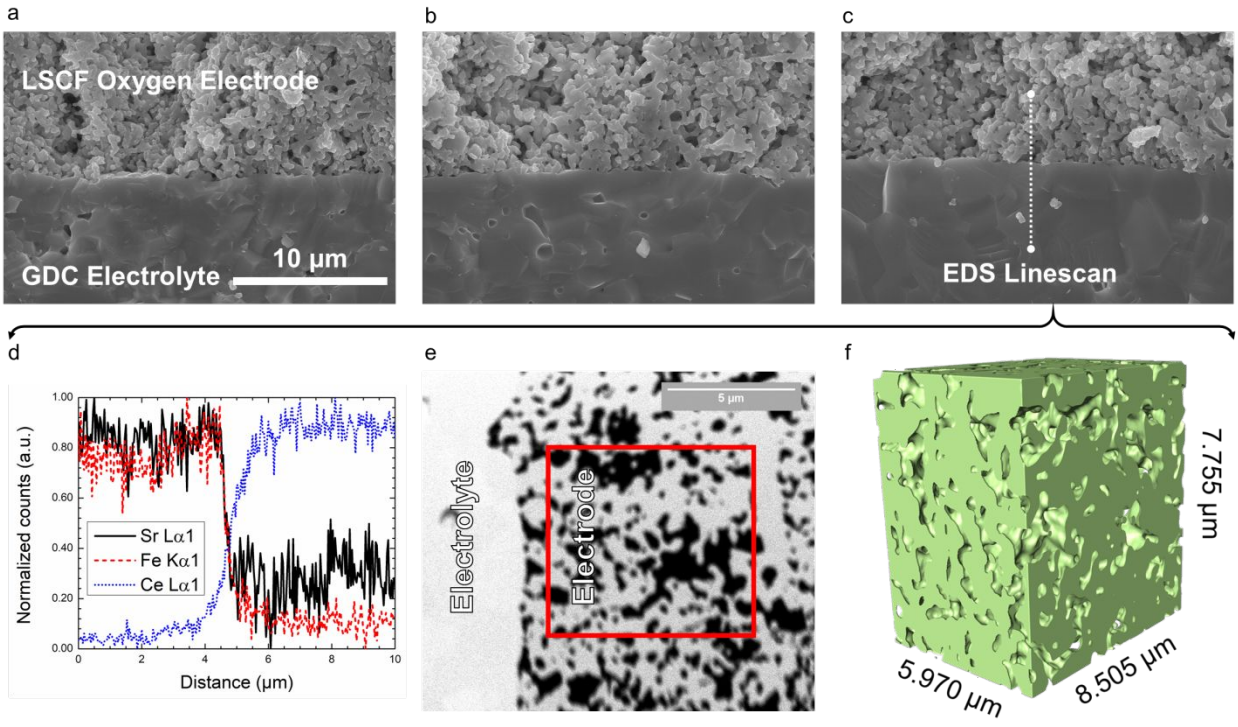

Fig. 5 | Microstructural characterization of LSCF electrodes and GDC electrolytes. a-c, SEM images of the electrode-electrolyte interface for samples: (**a**) untested control, (**b**) 650 °C with j = 1.5 A·cm^{-2} for 990 hours, (**c**) 750 °C with j = 1.5 A·cm^{-2} for 1013 hours. **d**, EDS result from **c**. **e**, FIB-SEM 2-D cross-section used to reconstruct **f**, a 3-D microstructure of **c**.

FIB-SEM is used to image an LSCF electrode after 1013 hours at 750 °C and j = 1.5 A·cm^{-2}. Figure 5f shows a typical FIB-SEM two-dimensional (2-D) cross-section from a series of images used to obtain the three-dimensional (3-D) tomographic image shown in Figure 5f. Only LSCF and pore phases are observed, with no evidence of Sr-rich clusters in the LSCF

150 electrode in Figures 5, which are sometimes observed after LSCF life testing at higher
151 temperatures.[45] These results can be compared directly with microstructural data from identically
152 prepared cells reported previously.[9,45] Table 1 compares porosity, surface area, and tortuosity
153 values obtained from the 3-D data sets for the present cell and prior cells, including a control cell
154 and cells tested for ~ 1000 hours at 700 °C with different current densities. The porosities fall in
155 the range between 35 to 40% and the tortuosities are in the expected range for such porosity
156 values. The variations between these values are small enough to be explained by cell-to-cell
157 differences and 3-D tomography measurement errors.[47,48] The specific surface area reductions
158 after the j = 1.5 A·cm^{-2} life tests are too small to draw a conclusion based on these results alone.
159 However, the results are consistent with a prior report showing coarsening at 700 °C and j = 1.5
160 A·cm^{-2}.[9] In any case, the observed amount of coarsening is not sufficient to significantly impact
161 R_P.[45,47]

162 Table 1 – **FIB-SEM results for LSCF|GDC|LSCF cells**. Porosity, tortuosity, and specific
163 surface areas calculated from the 3-D reconstruction and compared with prior literature results.

	Control (45)	**700 °C 0 A·cm^{-2}** (9)	**700 °C 0.7 A·cm^{-2}** (9)	**700 °C 1.5 A·cm^{-2}** (9)	**750°C 1.5 A·cm^{-2}**
Porosity (%)	33.1%	39.69%	39.59%	34.03%	35.33%
LSCF Tortuosity	1.10	1.12	1.12	1.10	1.35
Specific Surface Area (μm^{-1})	4.95	5.62	5.96	4.47	4.41

164

165 Sr Segregation

166 Figure 6 presents the amounts of excess Sr, normalized to the FIB-SEM-measured LSCF
167 surface areas, measured after various life tests compared with an untested control electrode. The
168 Sr amount does not increase after thermal annealing at 650 °C for 990 hours. However, Sr

coverages generally increase with increasing j at 650 °C, in agreement with prior reports that current accelerates Sr out-diffusion.[9,19,45] At j = 1.5 A·cm^{-2} the segregation is fast enough that R_P has increased substantially and then nearly stabilized by the end of the 650 °C life test. Previously-reported results for similar LSCF electrodes at 700 °C show that the surface Sr amount also increases with increasing j, but the amounts are larger than at 650 °C because of the faster Sr segregation at the higher temperature.[9] At 750 °C, there is a substantial increase in surface Sr after annealing for 1000 hours; as expected, Sr out-diffusion is faster at the higher temperature. Increasing to j at 750 °C further increases the amount of surface Sr, except at j = 1.5 A·cm^{-2} where the surface Sr declines. However, this slight decrease in segregation does not appear to be significant enough to explain the stable performance. The correlation between Sr segregation and the electrochemical performance is discussed further below.

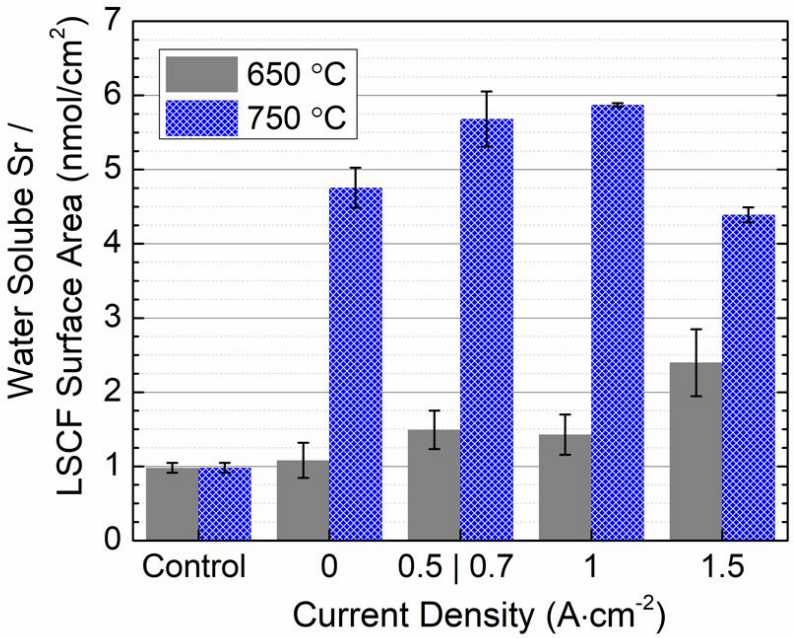

Fig. 6 | ICP-OES analysis of water soluble Sr in LSCF electrodes. The amount of segregated Sr species is normalized to the LSCF electrode surface area at 650 and 750 °C after testing for ~ 1000 hours with j = 0, 0.5, 0.7, 1.0, or 1.5 A·cm^{-2}.

Surface Cleaning

Figure 7 shows the resistance versus time for a cell that was first maintained without current for 999 hours at 750 °C, yielding a substantial increase in R_P over the first ~ 500 hours, in accord with the above results. The cell was then cooled to ambient temperature and rinsed in ultrapure H_2O. While this method is applicable to lab-scale symmetric electrodes that can be easily submersed in H_2O, there would likely be engineering challenges to introduce this cleaning step in a fuel cell stack. After drying and reheating the cell to 750 °C, the life test is resumed – the R_P value has reset to its initial un-degraded value, but then increases similar to the first ~ 500 hours of the test. Four separate cleaning steps are carried out using this procedure. After each wash, the R_P returns to its initial low value followed by degradation. The reset in R_P is also well represented as a reset of the Nyquist and Bode plots shown in Supplementary Fig. 2, where each wash effectively reverses the degradation in the Gerischer element. To ensure that the thermal cycling carried out as part of these measurements did not affect the results, the cell was removed at 1497 hours and subsequently ramped back to temperature without a washing step and no change in cell performance is seen. Given that the ultrapure H_2O wash is known to remove excess Sr, but not other cations,[19,45] these results clearly links the increases in R_P with Sr segregation. That is, the electrochemical degradation in Figures 1-4 results from Sr segregation.

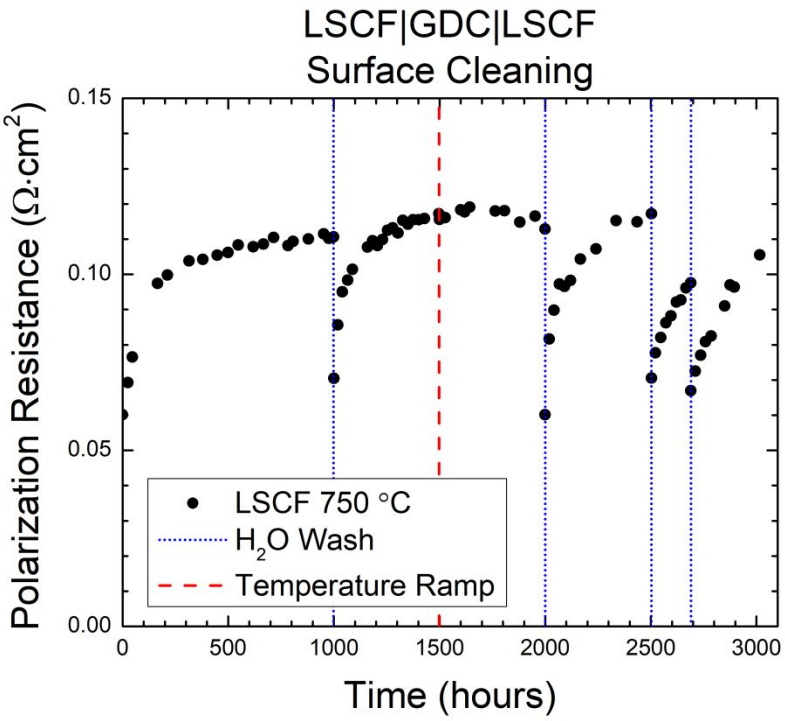

Fig. 7 | Polarization resistance over time for LSCF|GDC|LSCF cells using H_2O to remove surface segregated Sr. Cells are annealed at 750 °C with j = 0 A·cm^{-2} and washed with ultrapure water after 999, 2000, 2503, and 2690 hours.

Discussion

The results above show no evidence of interface microstructural degradation such as fracture, nor any increase ohmic resistance during the life tests. Such degradation, which has been widely observed in LSM-electrode SOCs operated in electrolysis and reversible modes,[11,49,50] is attributed to an oxygen pressure buildup at the interface associated with the electrode overpotential η.[51,52] These LSCF results agree with prior reports for LSCF-electrode cells reversibly-operated at 700 C and 1.0 A cm^{-2}, where the lack of interfacial degradation was explained by relatively low η values resulting from the low R_P values of LSCF electrodes.[9] The present results extend this observation to lower temperature and higher current density. They also more strongly confirm the conclusion from that study,[9] that electrochemical degradation is

associated with a Sr-enriched surface layer that impedes the oxygen surface exchange reaction, appearing in the EIS data as an increased Gerischer resistance.[9,44,45] This conclusion is consistent with prior surface spectroscopy studies on model $La_{0.6}Sr_{0.4}CoO_{3-\delta}$ and $La_{0.6}Sr_{0.4}Co_{0.2}Fe_{0.8}O_{3-\delta}$ thin film electrodes that show the development of a Sr-enriched perovskite surface at lower temperatures (400 to 650 °C). At higher temperatures, the Sr layer thickness covering the LSCF surface saturates while larger Sr islands nucleate.[53–57]

The above arguments, by themselves, do not explain the results in Figures 3 and 4, particularly the stable electrode operation at 750 C and 1.5 A cm^{-2}. These figures can be explained by noting (1) that increasing j increases the rate of surface segregation and (2) that the LSCF electrode exists in different states with different R_G depending on its history.[53–57] A cleaner electrode surface has a lower R_G, whereas the Sr segregated surface has a higher R_G. For example, in Figure 4b (j = 0 A·cm^{-2}), the initial R_G values are lower at higher temperature, as expected for activated electrode processes, because the LSCF surfaces are all in the clean state. Later in the life test, the 650 °C surface has clearly remained in the clean low R_G state due to slow Sr segregation, whereas at 700 and 750 °C R_G has increased due to accelerated Sr segregation.[19] This yields an unusual case where R_G at 650 °C is similar to that at 750 °C. The situation is reversed in Figure 4d (j = 1.5 A·cm^{-2}) because the current accelerates segregation. At 750 °C and 1.5 A·cm^{-2}, segregation is apparently so fast that a saturation Sr coverage has already been reached by the initial EIS measurement. Thus, the initial R_G is relatively high compared to the initial values at 650 and 700 °C where the surfaces are still clean. Later in the test, current-enhanced Sr segregation also increases R_G at 650 and 700 °C, such that the R_G values follow the temperature dependence expected for Sr-covered LSCF.

The present results on reversible operation do not provide direct information on stability during electrolysis or fuel cell operation. However, the present trend of improved stability at higher temperature seems consistent with prior electrolysis results – in higher temperature (> 750 °C) electrolysis tests with up to j = 1 A·cm^{-2} where the LSCF electrode appears to be reasonably stable,[16,30–34] whereas in lower temperature (≤ 700 °C) electrolysis with j = 0 to 1.5 A·cm^{-2}, where cation segregation causes serious degradation.[9,37,43,58,59] The present results suggest that at higher temperatures, Sr segregation occurs relatively quickly, and even with surface Sr present R_P values are low enough for good cell performance. In this case, the segregation-induced resistance increases may be viewed as an initial break-in process rather than degradation. At lower temperatures, Sr segregation is slower with relatively long times to reach saturation coverage,[19,45] causing gradual R_P increases. The saturation R_P values for Sr-covered LSCF may be too high to achieve desired power densities at these lower operating temperatures. It is unclear if a specific part of the reversing current cycle – fuel cell or electrolysis mode – is responsible for the observed acceleration of Sr segregation and associated degradation in LSCF electrodes.[9,11] A number of studies have shown that anodic polarization of ABO_3 oxygen electrodes during electrolysis operation exacerbates segregation by promoting the diffusion of cations towards the surface,[21–23,29] while a cathodic bias during fuel cell operation enhances cation diffusion away from the surfaces and into the bulk.[23,24,29] However, other studies have reported the opposite trend where extensive cation segregation is seen under cathodic polarization conditions.[25–28] Thus, it is unclear whether increasing the fraction of the cycle in fuel cell versus electrolysis mode would reduce electrode degradation, as reported in one prior study.[11]

In summary, degradation of LSCF electrode performance during reversing current operation is dominated by Sr segregation. Higher current densities accelerate Sr segregation,

increasing the rate of electrochemical performance degradation for lower operating temperatures (≤ 700 °C) where segregation is normally slow. At 750 °C, Sr segregation kinetics are faster such that Sr surface coverage saturates rapidly, especially with the accelerating effects of current. There is no degradation after a stable Sr surface layer is achieved, which occurs almost immediately at j = 1.5 A·cm^{-2}, and the electrochemical activity of LSCF at 750 °C is high enough to yield excellent performance. Cleaning the LSCF surface to remove segregated surface Sr effectively reduces the polarization resistance, but only temporarily until Sr resurfaces.

Methods

Symmetric oxygen electrode cells were prepared by dry pressing GDC powder (Rhodia) and sintering at 1450 °C for 6 hours. LSCF (Praxair) electrodes were screen printed (Heraeus V-737) on either side and fired at 1100 °C for 2 hours to achieve ~ 15 μm thick porous electrodes. LSM (Praxair) pellets and ink (Heraeus V-737) were used as electrical contacts rather than precious metal contacts to avoid possible contamination in the electrode.[60,61] Current direction was switched every 6 hours, giving a 12 hour period using a LabView controlled Keithley sourcemeter; current density (j) values indicated below denote the reversing current density. Some life tests were repeated to ensure their reproducibility.

Potentiostatic electrochemical impedance spectroscopy (EIS) measurements were taken in air at the operational temperature with no applied potential and a 20 mV perturbation using a Zahner IM6 Electrochemical Workstation. Prior to the impedance measurement, the current was stopped and the EIS measurement taken after ~ 15 minutes to allow the cell to stabilize. The impedance spectra were fit to an equivalent circuit model with an inductor, resistor, RQ element (high frequency), and Gerischer element (low frequency) in series. The Gerischer follows a form used by Railsback et al.[38] The complex nonlinear least squares fitting was performed using

ravdav software.[46] Scanning electron microscopy and energy dispersive X-ray spectroscopy were conducted using a Hitachi SU8030 field emission SEM. Samples were fractured and coated in 15 nm of Osmium to reduce charging.

Samples were infiltrated with epoxy and polished for focused-ion beam scanning electron microscopy (FIB-SEM). An FEI Helios and dual-beam Zeiss 1540XB with an accelerating voltage of 2 kV and a backscattered electron detector was used to take serial cross-sectional images. Segmentation and 3D reconstruction methods are described elsewhere.[62]

Inductively coupled plasma-optical emission spectroscopy (ICP-OES) analysis was used to measure segregated Sr-rich species. Three fragments from each cell were measured to improve the statistical accuracy of the results. The cells were stirred in ultrapure water for 30 minutes, which selectively dissolves Sr containing species allowing a measurement of the amount of Sr segregation.[19,44,45] The same electrodes were then dissolved in HCl overnight, providing a measure of the total amount of electrode material. The solutions are mixed with appropriate amounts of water, HCl, and HNO_3 for ICP-OES analysis using a Thermo iCAP 7600.

Since segregated Sr species (SrO, $Sr(OH)_2$, $SrCO_3$, etc.) are water soluble and LSCF is not,[55] H_2O is used to clean the LSCF surfaces rather than HCl, HNO_3, or HF. Previous studies have used these strong acids to etch the top surface of the perovskite electrode to expose a clean surface from deeper in the electrode, thereby improving electrochemical performance.[63–66] This technique is effective, but it is destructive and highly sensitive to time and the quantity of acid used. To clean the surface, cells ramp slowly from operating temperature to room temperature, rinsed in ultrapure H_2O for one minute, dried at 150 °C, and finally ramped back to temperature for annealing and electrochemical testing.

References

1 IRENA and CPI, *Global Landscape of Renewable Energy Finance 2018*, 2018.

2 Z. Yang, J. Zhang, M. C. W. Kintner-Meyer, X. Lu, D. Choi, J. P. Lemmon and J. Liu, *Chem. Rev.*, 2011, **111**, 3577–3613.

3 A. Pesaran, C. Ban, L. Cao, P. Graf, M. Keyser, G. Kim, S. Santhanagopalan, A. Saxon, Y. Shi, K. Smith, R. Tenent, A. Pesaran, C. Ban, L. Cao, P. Graf, M. Keyser, G. Kim, S. Santhanagopalan, A. Saxon, Y. Shi, K. Smith and R. Tenent, *Energy Storage Annual Progress Report for FY15*, 2016.

4 S. H. Jensen, C. Graves, M. Mogensen, C. Wendel, R. Braun, G. Hughes, Z. Gao and S. A. Barnett, *Energy Environ. Sci.*, 2015, **8**, 2471–2479.

5 D. M. Bierschenk, J. R. Wilson and S. A. Barnett, *Energy Environ. Sci.*, 2011, **4**, 944–951.

6 C. H. Wendel and R. J. Braun, *Appl. Energy*, 2016, **172**, 118–131.

7 R. Knibbe, M. L. Traulsen, A. Hauch, S. D. Ebbesen and M. Mogensen, *J. Electrochem. Soc.*, 2010, **157**, B1209–B1217.

8 G. A. Hughes, K. Yakal-Kremski, A. V. Call and S. A. Barnett, *J. Electrochem. Soc.*, 2012, **159**, F858–F863.

9 J. G. Railsback, H. Wang, Q. Liu, M. Y. Lu and S. A. Barnett, *J. Electrochem. Soc.*, 2017, **164**, F3083–F3090.

10 G. A. Hughes, K. Yakal-Kremski and S. A. Barnett, *Phys. Chem. Chem. Phys.*, 2013, **15**, 17257.

11 C. Graves, S. D. Ebbesen, S. H. Jensen, S. B. Simonsen and M. B. Mogensen, *Nat. Mater.*, 2015, **14**, 239–244.

12 K. Chen and S. P. Jiang, *J. Electrochem. Soc.*, 2016, **163**, F3070–F3083.

13 J. Kim, H. Il Ji, H. P. Dasari, D. Shin, H. Song, J. H. Lee, B. K. Kim, H. J. Je, H. W. Lee

and K. J. Yoon, *Int. J. Hydrogen Energy*, 2013, **38**, 1225–1235.

14 A. Momma, T. Kato, Y. Kaga and S. Nagata, *J. Ceram. Soc. Japan*, 1997, **105**, 369–373.

15 V. Brichzin, J. Fleig, H. Habermeier, G. Cristiani and J. Maier, 2002, **153**, 499–507.

16 V. N. Nguyen, Q. Fang, U. Packbier and L. Blum, *Int. J. Hydrogen Energy*, 2013, **38**, 4281–4290.

17 D. Ferrero, A. Lanzini, P. Leone and M. Santarelli, *Chem. Eng. J.*, 2015, **274**, 143–155.

18 E. Oh, Dongjo, Gostovic, Danijel, Wachsman, *J. Mater. Res.*, 2012, **27**, 4–11.

19 H. Wang and S. A. Barnett, *ECS Trans.*, 2017, **78**, 905–913.

20 W. Lee, J. W. Han, Y. Chen, Z. Cai and B. Yildiz, *J. Am. Chem. Soc.*, 2013, **135**, 7909–7925.

21 Y. Li, W. Zhang, Y. Zheng, J. Chen, B. Yu, Y. Chen and M. Liu, *Chem. Soc. Rev.*, 2017, **46**, 6345–6378.

22 Y. Liu, K. Chen, L. Zhao, B. Chi, J. Pu, S. P. Jiang and L. Jian, *Int. J. Hydrogen Energy*, 2014, **39**, 15868–15876.

23 A. K. Huber, M. Falk, M. Rohnke, B. Luerssen, M. Amati, L. Gregoratti, D. Hesse and J. Janek, *J. Catal.*, 2012, **294**, 79–88.

24 M. Finsterbusch, A. Lussier, J. A. Schaefer and Y. U. Idzerda, *Solid State Ionics*, 2012, **212**, 77–80.

25 Z. He, L. Zhang, S. He, N. Ai, K. Chen, Y. Shao and S. Ping, *J. Power Sources*, 2018, **404**, 73–80.

26 S. He, M. Saunders, K. Chen, H. Gao, A. Suvorova, W. D. A. Rickard, Z. Quadir, C. Q. Cui and S. P. Jiang, *J. Electrochem. Soc.*, , DOI:10.1149/2.0151807jes.

27 N. Ai, S. He, N. Li, Q. Zhang, W. D. A. Rickard, K. Chen, T. Zhang and S. P. Jiang, *J.*

Power Sources, 2018, **384**, 125–135.

28 E. Mutoro, E. J. Crumlin, H. Pöpke, B. Luerssen, M. Amati, M. K. Abyaneh, M. D. Biegalski, H. M. Christen, L. Gregoratti, J. Janek and Y. Shao-Horn, *J. Phys. Chem. Lett.*, 2012, **3**, 40–44.

29 A.-K. Huber, M. Falk, M. Rohnke, B. Luerßen, L. Gregoratti, M. Amati and J. Janek, *Phys. Chem. Chem. Phys.*, 2012, **14**, 751–758.

30 F. Tietz, D. Sebold, A. Brisse and J. Schefold, *J. Power Sources*, 2013, **223**, 129–135.

31 D. The, S. Grieshammer, M. Schroeder, M. Martin, M. Al Daroukh, F. Tietz, J. Schefold and A. Brisse, *J. Power Sources*, 2015, **275**, 901–911.

32 F. Tietz, V. A. C. Haanappel, A. Mai, J. Mertens and D. Stöver, *J. Power Sources*, 2006, **156**, 20–22.

33 J. Schefold, A. Brisse and F. Tietz, *J. Electrochem. Soc.*, 2012, **159**, A137.

34 J. Schefold, A. Brisse and H. Poepke, *Int. J. Hydrogen Energy*, 2017, **42**, 13415–13426.

35 K. Chen, S.-S. Liu, N. Ai, M. Koyama and S. P. Jiang, *Phys. Chem. Chem. Phys.*, 2015, **17**, 31308–15.

36 S. Y. Gomez and D. Hotza, *Renew. Sustain. Energy Rev.*, 2016, **61**, 155–174.

37 L. V. Mogni, K. Yakal-Kremski, C. M. Chanquía, Z. Gao, H. Wang, A. Caneiro and S. A. Barnett, *ECS Trans.*, 2015, **66**, 169–176.

38 J. Railsback, G. Hughes, L. Mogni, A. Montenegro-Hernández and S. Barnett, *J. Electrochem. Soc.*, 2016, **163**, F1433–F1439.

39 N. Hildenbrand, P. Nammensma, D. H. A. Blank, H. J. M. Bouwmeester and B. A. Boukamp, *J. Power Sources*, 2013, **238**, 442–453.

40 F. S. Baumann, J. Fleig, H. U. Habermeier and J. Maier, *Solid State Ionics*, 2006, **177**,

1071–1081.

41 D. Marinha, L. Dessemond, J. S. Cronin, J. R. Wilson, S. A. Barnett and E. Djurado, *Chem. Mater.*, 2011, **23**, 5340–5348.

42 Z. Pan, Q. Liu, L. Zhang, X. Zhang and S. H. Chan, *Electrochim. Acta*, 2016, **209**, 56–64.

43 X. Lou, S. Wang, Z. Liu, L. Yang and M. Liu, 2009, **180**, 1285–1289.

44 H. Wang, K. J. Yakal-Kremski, T. Yeh, G. M. Rupp, A. Limbeck, J. Fleig and S. A. Barnett, *J. Electrochem. Soc.*, 2016, **163**, F581–F585.

45 H. Wang and S. A. Barnett, *J. Electrochem. Soc.*, 2018, **165**, F564–F570.

46 C. Graves, 2012.

47 E. Lay-Grindler, J. Laurencin, J. Villanova, I. Kieffer, F. Usseglio-Viretta, T. Le Bihan, P. Bleuet, A. Mansuy and G. Delette, *ECS Trans.*, 2013, **57**, 3177–3187.

48 J. Scott Cronin, K. Muangnapoh, Z. Patterson, K. J. Yakal-Kremski, V. P. Dravid and S. A. Barnett, *J. Electrochem. Soc.*, 2012, **159**, B385.

49 M. A. Laguna-Bercero, R. Campana, A. Larrea, J. A. Kilner and V. M. Orera, *J. Power Sources*, 2011, **196**, 8942–8947.

50 M. S. Sohal, J. E. O'Brien, C. M. Stoots, V. I. Sharma, B. Yildiz and A. Virkar, *J. Fuel Cell Sci. Technol.*, 2012, **9**, 011017.

51 A. V. Virkar, J. Nachlas, A. V. Joshi and J. Diamond, *J. Am. Ceram. Soc.*, 1990, **73**, 3382–3390.

52 A. V. Virkar, *Int. J. Hydrogen Energy*, 2010, **35**, 9527–9543.

53 Z. Cai, M. Kubicek, J. Fleig and B. Yildiz, *Chem. Mater.*, 2012, **24**, 1116–1127.

54 A. K. Opitz, C. Rameshan, M. Kubicek, G. M. Rupp, A. Nenning, T. Götsch, R. Blume, M. Hävecker, A. Knop, G. Rupprechter, B. Klötzer and J. Fleig, *Top. Catal.*, 2018, **61**,

2129–2141.

55 G. M. Rupp, A. K. Opitz, A. Nenning, A. Limbeck and J. Fleig, *Nat. Mater.*, 2017, **16**, 640–645.

56 G. M. Rupp, H. Tellez, J. Druce, A. Limbeck, T. Ishihara, J. Kilner and J. Fleig, *J. Mater. Chem. A*, 2015, **3**, 22759–22769.

57 N. J. Simrick, A. Bieberle-Hütter, T. M. Ryll, J. A. Kilner, A. Atkinson and J. L. M. Rupp, *Solid State Ionics*, 2012, **206**, 7–16.

58 R. R. Liu, S. H. Kim, S. Taniguchi, T. Oshima, Y. Shiratori, K. Ito and K. Sasaki, *J. Power Sources*, 2011, **196**, 7090–7096.

59 L. Blum, L. G. J. de Haart, J. Malzbender, N. Margaritis and N. H. Menzler, *Energy Technol.*, 2016, **4**, 939–942.

60 S. P. Simner, M. D. Anderson, L. R. Pederson and J. W. Stevenson, *J. Electrochem. Soc.*, 2005, **152**, A1851.

61 K. Yakal-Kremski, G. A. Hughes, A. V Call and S. A. Barnett, *ECS Trans.*, 2012, **41**, 129–136.

62 J. S. Cronin, J. R. Wilson and S. A. Barnett, *J. Power Sources*, 2011, **196**, 2640–2643.

63 W. Jung and H. L. Tuller, *Energy Environ. Sci.*, 2012, **5**, 5370–5378.

64 S. P. Jiang and J. G. Love, *Solid State Ionics*, 2001, **138**, 183–190.

65 W. Wang and S. P. Jiang, *Solid State Ionics*, 2006, **177**, 1361–1369.

66 M. Kubicek, A. Limbeck, T. Frömling, H. Hutter and J. Fleig, *J. Electrochem. Soc.*, 2011, **158**, B727.

Acknowledgements

This material is based upon work supported by the National Science Foundation under grant no. OISE-1545907 and DMR-1506925. Shan-Lin Zhang gratefully acknowledges the scholarship from the State Scholarship Fund of China Scholarship Council (201606285002). This work made use of the EPIC facility of Northwestern University's NUANCE Center, which has received support from the Soft and Hybrid Nanotechnology Experimental (SHyNE) Resource (NSF ECCS-1542205); the MRSEC program (NSF DMR-1121262) at the Materials Research Center; the International Institute for Nanotechnology (IIN); the Keck Foundation; and the State of Illinois, through the IIN. This work made use of the MatCI Facility which receives support from the MRSEC Program (NSF DMR-1720139) of the Materials Research Center at Northwestern University. Metal analysis was performed at the Northwestern University Quantitative Bio-element Imaging Center. The authors would like to thank Roberto Scipioni with assistance using ravdav software and Travis A. Schmauss, David Lam, Allessandra DiCorato, and Cesar Villa for assistance with ICP-OES sample preparation.

Author contributions

M.Y.L., J.G.R., and S.A.B. planned the experiments and analyzed the data. M.Y.L., J.G.R., H.W., and Y.A.C. fabricated samples. M.Y.L., J.G.R., H.W., Y.A.C., and S.Z. performed electrochemical measurements. M.Y.L., H.W., and Q.L. contributed to ICP-OES and FIB-SEM. M.Y.L. and Y.A.C. took SEM images. M.Y.L. and S.A.B. wrote the manuscript. S.A.B. developed and supervised the project.

Competing interests

The authors declare no competing interests.

Correspondence and requests for materials should be addressed to S.A.B.

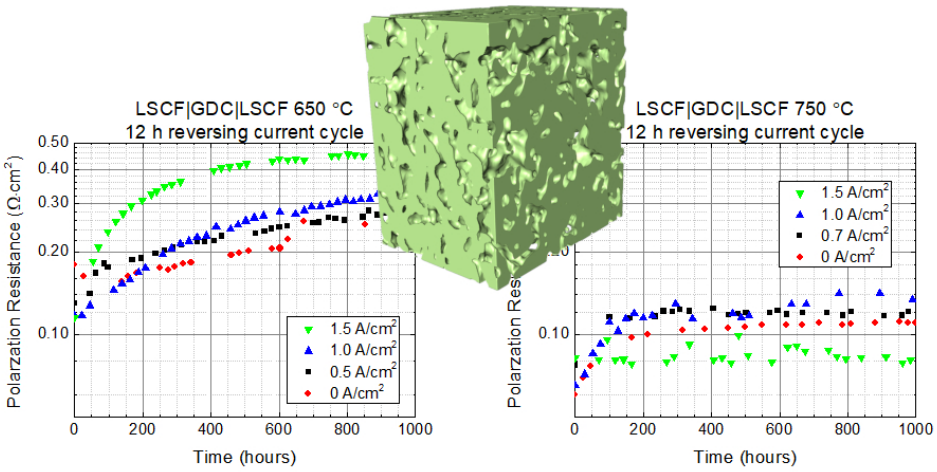

80x39mm (300 x 300 DPI)

Stable operation of LSCF oxygen electrodes with high current densities at high temperatures for solid oxide electrochemical cells